Comput Visual Sci 7: 199–206 (2004)
Digital Object Identifier (DOI) 10.1007/s00791-004-0150-3

Computing and Visualization in Science

Regular article

Nonlinear multigrid methods for total variation image denoising

Claudia Frohn-Schauf[1], **Stefan Henn**[2], **Kristian Witsch**[2]

[1] Institut für Medizin, Forschungszentrum Jülich GmbH, 52425 Jülich, Germany
(e-mail: frohn@am.uni-duesseldorf.de)
[2] Mathematisches Institut, Heinrich-Heine Universität Düsseldorf, 40225 Düsseldorf, Germany
(e-mail: {henn, witsch}@am.uni-duesseldorf.de, http://www.am.uni-duesseldorf.de/∼henn, http://www.am.uni-duesseldorf.de/∼witsch)

Received: 31 January 2003 / Accepted: 26 March 2004
Published online: 31 August 2004 – © Springer-Verlag 2004

Communicated by: G. Wittum

Abstract. The classical image denoising technique introduced by Rudin, Osher, and Fatemi [17] a decade ago, leads to solve a constrained minimization problem for the total variation (*TV*) of the image. The formal first variation of the minimization problem is a nonlinear and highly anisotropic boundary value problem. In this paper, a computational PDE method based on a nonlinear multigrid scheme for restoring noisy images is suggested. Here, we examine different discretizations for the Euler–Lagrange equation as well as different smoothers within the multigrid scheme. Then we describe the iterative total variation regularization scheme, which starts with an isotropic ("smooth") problem and leads to smooth edges in the image. Within the iteration the problem becomes more and more anisotropic and converges to an image with sharp edges. Finally, we present some experimental results for synthetic and real images.

1 Introduction

Image denoising is the process of reconstructing an unknown image $u(x, y)$ from given data $z(x, y)$ satisfying

$$z(x, y) = u(x, y) + \eta(x, y)\,. \tag{1}$$

Here, $\eta(x, y)$ is an additive noise, which is usually assumed to be random with known mean value zero and variance σ^2. In order to compute meaningful solutions we use regularizing techniques that incorporate additional information about the image $u(x, y)$. Tikhonov H^1 regularization, which aims at smooth solutions, is poorly when $u(x, y)$ includes discontinuities or steep gradients. The model proposed by Rudin, Osher, and Fatemi [17] leads us to choose the total variation $TV[u] = \int_\Omega |\nabla u| d\Omega$ or a smooth approximation $TV_\beta[u]$ with a smoothing parameter β and to search for a solution among the minima of the functional

$$J_{\alpha,\beta}[u(x, y)] = ||u(x, y) - z(x, y)||^2_{L_2(\Omega)} + \alpha TV_\beta[u(x, y)]\,, \tag{2}$$

which penalizes the total variation of the image u.

The parameter $\alpha \in \mathbb{R}^+$ allows us to balance the influence of both terms in the functional, and the larger β the smoother the problem.

To solve the *TV*-penalized image denoising problem Rudin et al. [17] used an artificial time marching technique. Vogel and Oman [23] used a relaxed fixed point iteration, which is speeded up by a multigrid correction scheme as inner iteration (see [15]) and requires in general many iterations (e.g., see [21], 400 multigrid iterations). The application of a primal dual version of Newtons method is presented in [7]. Chan et al. [6] combine Newtons method with a continuation scheme for β. Li and Santosa [14] have developed an alternative algorithm for this problem based on interior point methods for convex optimization.

This paper is organized as follows. First, in Sect. 2 we will present more precisely the minimization problem studied here, as well as the assumptions to impose on the model. For the minimization of the functional in Sect. 3 a nonlinear multigrid method in the form of the full approximation scheme (FAS) is applied. Additionally we will analyze the behavior of the FAS dependent on the underlying norm in $TV[u]$ as well as on different smoothers and transfer operators within the FAS.

A minimizer of the image denoising functional (2) depends significantly on the choice of the parameter β. In the solution process β plays a dual role. First, it can be regarded as a smoothing or regularization parameter. Second, it can be considered as a continuation parameter [6]. Theoretically, decreasing β should give a better approximation of the total variation (e.g., see [1]), but in practice a too small β leads to strong anisotropic and nearly degenerated PDE's which are difficult to solve.

Increasing β removes these anisotropies and aims at smooth solutions similar to the L_2 case. In Sect. 4, we present

an algorithm which successively reduces the parameter β within a sequence of minimization problems.

2 The image denoising problem

In order to restore the image u we have to solve (1) for u. To compensate for the absence of information in (1), one must apply methods which retain desired features to the solution. This is done usually in the form of a smoothness assumption, i.e. it is assumed that $\int_\Omega |\nabla u(x, y)|^2 dxdy$ is small. This leads us to solve the constrained minimization problem

$$\min_u \int_\Omega |\nabla u|^2 dxdy \quad s.t. \quad ||u - z||^2 = \sigma^2 .$$

An equivalent approach is to use a Lagrange multiplier α and to solve the unconstrained minimization problem

$$\min_u \left\{ \int_\Omega (u(x, y) - z(x, y))^2 dxdy + \alpha \int_\Omega |\nabla u(x, y)|^2 dxdy \right\} .$$

This kind of regularization is known as Tikhonov H^1 regularization (see, e.g. [2, 10]). Tikhonov H^1 regularization, which aims at smooth solutions, is poorly when u includes discontinuities or steep gradients, cf. Figs. 1–2. The model proposed by Rudin, Osher, and Fatemi [17] leads us to choose the total variation of the image u

$$TV[u] = \int_\Omega |\nabla u| dxdy = \int_\Omega \sup_{||v|| \le 1} \nabla u^T \cdot v dxdy$$

Fig. 1. *Left*: Original image u (128×128 pixels). *Right*: Image $z = u +$ Gaussian white noise

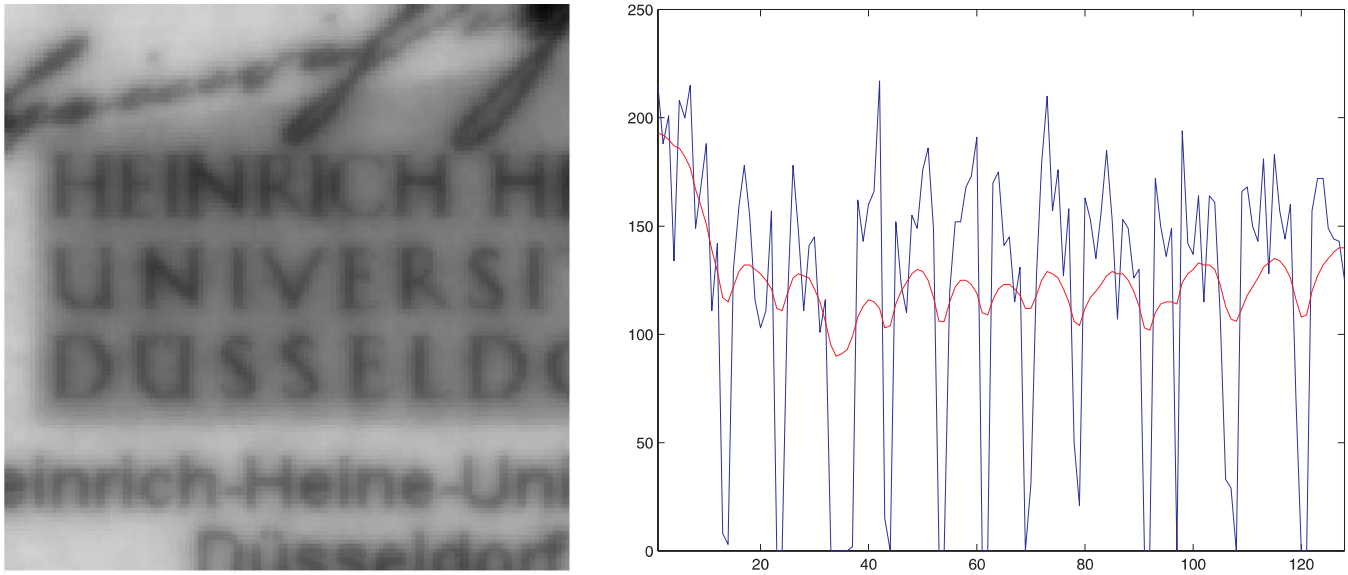

Fig. 2. *Left:* Result found with Tikhonov H^1 regularization. *Right:* Functional representation of the image row 60 of the noisy image z (*blue*) and the resulting image u (*red*) displayed *left*

$$= \int_\Omega \sup_{||v|| \le 1} (u_x \cdot v_1 + u_y \cdot v_2) dxdy \,.$$

This yields

$$TV[u] = \int_\Omega |u_x| + |u_y| \, dxdy = \int_\Omega \sqrt{u_x^2} + \sqrt{u_y^2} \, dxdy$$

if $||\cdot|| = ||\cdot||_1$ and

$$TV[u] = \int_\Omega \sqrt{u_x^2 + u_y^2} \, dxdy$$

for $||\cdot|| = ||\cdot||_2$.

The total variation idea can be traced back to shock capturing methods in Computational Fluid Dynamics (CFD). In image processing the total variation model can be used to model denoising, deblurring, as well as image inpainting (e.g. restoring old scabbed photos). Total variation methods in image processing were extensively studied during the last ten years, both theoretically and practically; in particular, well posedness is shown in [5]. Unfortunately the integrand is not differentiable where $\nabla u = 0$. In the literature several ways are suggested to overcome this problem. One approach is to regularize the functional itself by replacing its value near singularities by the usual L_2-Norm. Another method (see [16]) is to replace the gradient ∇ by a bounded operator L_h, so that the resulting functional becomes differentiable over $L_2(\Omega)$. The authors in [8] propose a wavelet based procedure which does not need any auxiliary regularization method. In this paper we use a common method (see e.g. [1]) which obtains a regularization by replacing the total variation $TV[u]$ by a smooth approximation

$$TV_\beta[u] = \begin{cases} \displaystyle\int_\Omega \sqrt{u_x^2 + \beta} + \sqrt{u_y^2 + \beta} \, dxdy & \text{if } |\cdot| = |\cdot|_1 \\ \displaystyle\int_\Omega \sqrt{u_x^2 + u_y^2 + \beta} \, dxdy & \text{if } |\cdot| = |\cdot|_2 \end{cases}$$

with a smoothing parameter $\beta > 0$. We search for a solution among the minima of the functional

$$J_{\alpha,\beta}[u] = ||u - z||^2_{L_2(\Omega)} + \alpha TV_\beta[u] \,. \tag{3}$$

According to the fundamental lemma of calculus of variations (cf. [9]) the formal first variation (Euler–Lagrange equation) of $J_{\alpha,\beta}[u]$ is given by the boundary value problem (cf. [22])

$$\left(\mathcal{L} + \frac{2}{\alpha} I\right) u(x, y) = \frac{2}{\alpha} z(x, y) \quad \text{for all } (x, y) \in \overline{\Omega}$$

$$\frac{\partial u(x, y)}{\partial n} = 0 \qquad \text{for all } (x, y) \in \partial\Omega \tag{4}$$

with the nonlinear differential operator

$$\mathcal{L}u(x, y) = \begin{cases} \operatorname{div}\left(\dfrac{\nabla u(x, y)}{\sqrt{u_x^2(x, y) + \beta} + \sqrt{u_y^2(x, y) + \beta}}\right) & \text{if } |\cdot| = |\cdot|_1 \\ \operatorname{div}\left(\dfrac{\nabla u(x, y)}{\sqrt{u_x^2(x, y) + u_y^2(x, y) + \beta}}\right) & \text{if } |\cdot| = |\cdot|_2 \,. \end{cases}$$

This nonlinear and highly anisotropic elliptic type equation must be solved numerically. Due to the typical image-size with up to $N_x \times N_y = 1024 \times 1024$ pixels or even more it is extremely important to use a very efficient solver. Methods which do not take into account the $\mathcal{O}(N^2)$ (where $N = \max(N_x, N_y)$) condition of the regularization term will have convergence rates strongly dependent on the number of picture elements.

3 Multigrid image denoising

Nonlinear multigrid methods can be used to provide efficient numerical solutions for the image denoising problem. In this section, a multigrid algorithm to solve the nonlinear

Fig. 3. Result found with iterative total variation regularization. *Left:* By using $||\cdot||_1$. *Right*: By using $||\cdot||_2$

and highly anisotropic PDE in (4) is presented and analyzed numerically. First, we introduce the discretization and approximation of the PDE. Then, for this discretization robust intergrid transfer functions and smoothing techniques for the multigrid algorithm are presented.

3.1 Discretization

Images are typically encoded as two-dimensional arrays. Each element in the matrix represents a pixel (picture element) with gray intensity between black and white (0 and 255).

The resulting image-array is a finite-dimensional approximation of a continuous image and is represented on a rectangular equidistant grid

$$g^h_{i,j} = \left(x_i, y_j\right) = \left(ih_x, jh_y\right) \in \overline{\Omega},\ 0 \le i \le N_x,\ 0 \le j \le N_y$$

with $(N_x + 1) \times (N_y + 1)$ grid points with pixel-wide h_x and pixel-height h_y given by

$$h = (h_x, h_y) = \left(N_x^{-1}, N_y^{-1}\right).$$

3.2 Approximation

Let $u^h_{i,j}$, $z^h_{i,j}$ and $|\nabla u^h_{i,j}|$ denote the grids of functions defined by $u^h_{i,j} = u(g^h_{i,j})$, $z^h_{i,j} = z(g^h_{i,j})$ and $|\nabla u^h_{i,j}| = |\nabla u(g^h_{i,j})|$ as well as their second-order finite difference approximations at staggered grid points

$$D_x^{\frac{h_x}{2}} u^h_{i+\frac{1}{2},j} = \left(u^h_{i+1,j} - u^h_{i,j}\right)/h_x$$

and

$$D_y^{\frac{h_y}{2}} u^h_{i,j+\frac{1}{2}} = \left(u^h_{i,j+1} - u^h_{i,j}\right)/h_y\,.$$

We can now replace the spatial derivatives in the operator $\mathcal{L}$ by their second-order finite difference approximations. For $||\cdot||_1$, the discretized differential operator $\mathcal{L}$ becomes

$$L^{[1]}_h = \begin{pmatrix} 0 & a^y_{i,j+\frac{1}{2}} & 0 \\ a^x_{i-\frac{1}{2},j} & \Sigma^{[1]}_{i,j} & a^x_{i+\frac{1}{2},j} \\ 0 & a^y_{i,j-\frac{1}{2}} & 0 \end{pmatrix}$$

with

$$a^x_{i,j} = \frac{h_x^{-2}}{\sqrt{\left(D_x^{\frac{h_x}{2}} u^h_{i,j}\right)^2 + \beta}},\quad a^y_{i,j} = \frac{h_y^{-2}}{\sqrt{\left(D_y^{\frac{h_y}{2}} u^h_{i,j}\right)^2 + \beta}} \tag{5}$$

and

$$\Sigma^{[1]}_{i,j} = -\left(a^x_{i-\frac{1}{2},j} + a^x_{i+\frac{1}{2},j} + a^y_{i,j-\frac{1}{2}} + a^y_{i,j+\frac{1}{2}}\right)$$

respectively for $||\cdot||_2$

$$L^{[2]}_h = \begin{pmatrix} 0 & a_{i,j+\frac{1}{2}} & 0 \\ a_{i-\frac{1}{2},j} & \Sigma^{[2]}_{i,j} & a_{i+\frac{1}{2},j} \\ 0 & a_{i,j-\frac{1}{2}} & 0 \end{pmatrix}$$

with

$$a_{i,j} = \frac{\left(h_x h_y\right)^{-1}}{\sqrt{\left(D_x^{\frac{h}{2}} u^h_{i,j}\right)^2 + \left(D_y^{\frac{h}{2}} u^h_{i,j}\right)^2 + \beta}} \tag{6}$$

and

$$\Sigma^{[2]}_{i,j} = -\left(a_{i-\frac{1}{2},j} + a_{i+\frac{1}{2},j} + a_{i,j-\frac{1}{2}} + a_{i,j+\frac{1}{2}}\right).$$

The resulting equation for all inner grid points $g^h_{i,j}$, e.g., for the $||\cdot||_1$ case is given by

$$\begin{pmatrix} 0 & a^y_{i,j+\frac{1}{2}} & 0 \\ a^x_{i-\frac{1}{2},j} & \Sigma^{[1]}_{i,j} + \dfrac{2}{\alpha} & a^x_{i+\frac{1}{2},j} \\ 0 & a^y_{i,j-\frac{1}{2}} & 0 \end{pmatrix} u^h_{i,j} = \frac{2}{\alpha} z^h_{i,j}\,.$$

Central second order approximations are used to approximate the outward normal of the boundary value problem (4) and to eliminate the external grid-points ("ghost-points") in the discretized differential operators $L^{[\nu]},\ \nu \in \{1, 2\}$. This leads, e.g., for $L^{[1]}$ to the following equation

$$\begin{pmatrix} 0 & a^y_{i,j+\frac{1}{2}} & 0 \\ a^x_{i-\frac{1}{2},j} + a^x_{i+\frac{1}{2},j} & \Sigma^{[1]}_{i,j} + \dfrac{2}{\alpha} & 0 \\ 0 & a^y_{i,j-\frac{1}{2}} & 0 \end{pmatrix} u^h_{i,j} = \frac{2}{\alpha} z^h_{i,j}$$

for grid-points at the right boundary.

This is a stable second order approximation of the boundary value problem (4), therefore we have second order convergence for smooth right hand side z, cf. [11].

The constants however depend on $\frac{1}{\sqrt{\beta}}$ and are large for small β. This is not really interesting in this situation: One wants reasonable discrete solutions with not too large total variation, not an approximation of a continuous solution.

3.3 Multigrid

With the Euler–Lagrange equation discretized by finite differences as described in the previous section, the nonlinear functional $TV_\beta[u]$ is naturally defined on the finest level with grid-size $h = (h_x, h_y)$ given by the pixel size $(N_x + 1, N_y + 1)$ of the image z (see Sect. 3.1). The basic idea of the multigrid full approximation scheme (FAS) for nonlinear problems ([3, 19]) is to smooth the errors of the solution in one or two smoothing steps such that they can be approximated on a coarser grid. Here we use standard coarsening, which means that we double the step length $h = (h_x, h_y)$ in x- and y-direction, so that the coarse image has a fourth of the pixels of the corresponding fine one. On the coarse grid, a nonlinear defect equation is solved and then the coarse grid corrections are interpolated back to the fine grid, where the errors are

smoothed again. This strategy is applied recursively down to the coarsest grid consisting of 9 grid points (only one inner grid point).

The FAS is characterized by the so-called multigrid-components. Designing a FAS for total variation image denoising has to be done carefully. One has to specify the multigrid-components to preserve steep edges. Straightforward multigrid-components may violate the intend of total variation image denoising.

3.3.1 Intergrid transfers. To use efficient solution methods like FAS for the nonlinear PDE we have to define the problem also on coarse grids. By coarsening the fine grid functions $u^h_{i,j}$ and $z^h_{i,j}$, a corresponding discrete problem can be defined also on the next coarser resolution. There are several possibilities for the intergrid transfer functions (see, e.g. [19]).

In principle, the images are coarsened by collecting several picture elements into one coarse picture element. Here to preserve steep edges, we use the injection operator

$$u^{2^{l+1}h}_{i,j} = u^{2^l h}_{2i,2j} \quad \text{for} \quad l = 0, 1, \ldots$$

to transform the images to a coarser resolution. I.e. we just take all pixel values that lie on the fine and the coarse grid as coarse grid values. In image processing this operator is simply a sampling scheme and corresponds to a lowpass filter for $u^h_{i,j}$. Applied recursively, this procedure yields a sequence of coarser and coarser images which contain only information about corresponding coarse structures.

For the coarse to fine transfer of the corrections we use bilinear interpolation.

3.3.2 Relaxation. During relaxation we must linearize our discretization. This is simply, but without damage done by the use of 'frozen coefficients' given in (5) and (6) resp., i.e. local linearization of the principal terms.

The choice of the relaxation method for the discrete image denoising problem is important in both the traditional relaxation – and multigrid solution methods. Here, the problem contains variable coefficients and the directions of strong and weak coupling are not known in advance or change inside the domain. So if we use a pointwise Gauss–Seidel scheme, we possibly go forward in the complete wrong direction, so that the maximum norm of the solution may not change in the first relaxation steps and we cannot achieve good smoothing in a few steps. For the image denoising problem, streaking artifacts have been observed when a classical pointwise smoothing scheme (e.g. pointwise Gauss–Seidel) is used.

Therefore, an alternating line Gauss–Seidel must be employed as a robust relaxation method, because in this method for all grid points of the considered line the equations are solved simultaneously. The alternating line Gauss–Seidel relaxation (ALR) in lexicographic order performs one sweep of line Gauss–Seidel relaxation along the x-coordinate direction, followed by another sweep of line Gauss–Seidel relaxation along the y-coordinate direction, see [3, 4, 20].

3.4 Numerical results

Consider the image displayed in Fig. 1. For this example, we will give some asymptotic rates of convergence, given by

$$\varrho := \lim_{k\to\infty} \frac{d\left(u^{k+1}\right)}{d\left(u^k\right)} \text{ (estimated)}.$$

For the nonlinear multigrid scheme the pointwise Gauss–Seidel (pGS(ω)) relaxation and the alternating line Gauss–Seidel (ALR(ω)) with an relaxing-parameter ω are compared. The rates become good (as expected) as long as β is greater or approximately equal to the radicand of the term within the total variation functional, i.e. $\sqrt{u_x^2}$, $\sqrt{u_y^2}$ or $\sqrt{u_x^2+u_y^2}$ on the different image resolutions. One consequence is that the multigrid scheme does not any longer converge in general when β becomes smaller than 10^3. We now turn our attention to the convergence rates dependent on the smoothing parameter β. The convergence results are shown in Table 1. By using the pointwise Gauss–Seidel relaxation we observe no convergence (n.c.) of the multigrid scheme for relatively small β. Note, that an ALR is approximately four times as expensive as a pointwise Gauss–Seidel relaxation in lexicographic

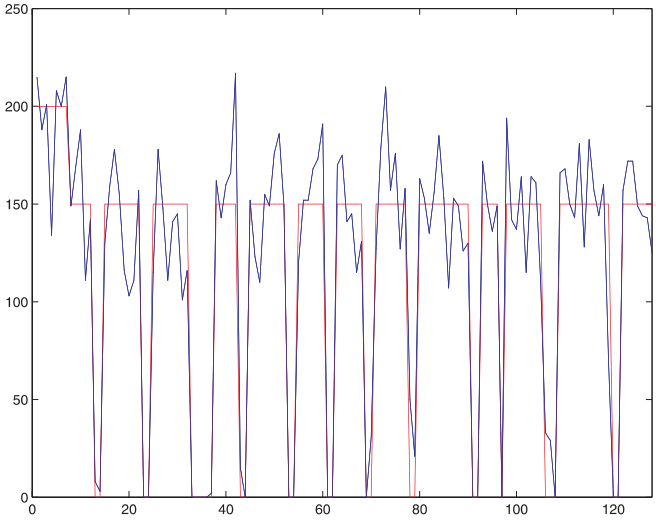

Fig. 4. Functional representation of the image row 60 of the noisy image z (*blue*) and the original image u (*red*) displayed in Fig. 1

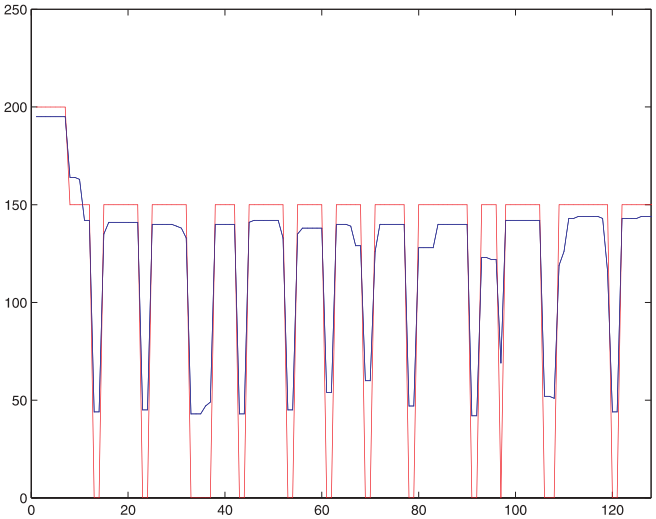

Fig. 5. Functional representation of the image row 60 of the original image u (*red*) and the result (by using $||\cdot||_1$) displayed in Fig. 3 left

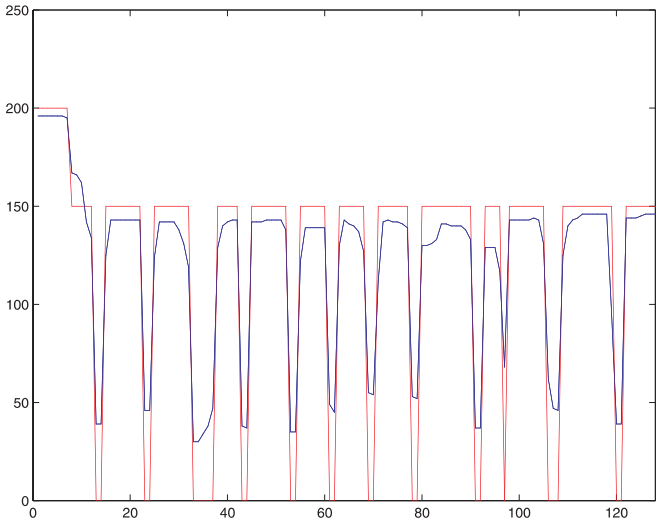

Fig. 6. Functional representation of the image row 60 of the original image u (*red*) and the result (by using $||\cdot||_2$) displayed in Fig. 3 right

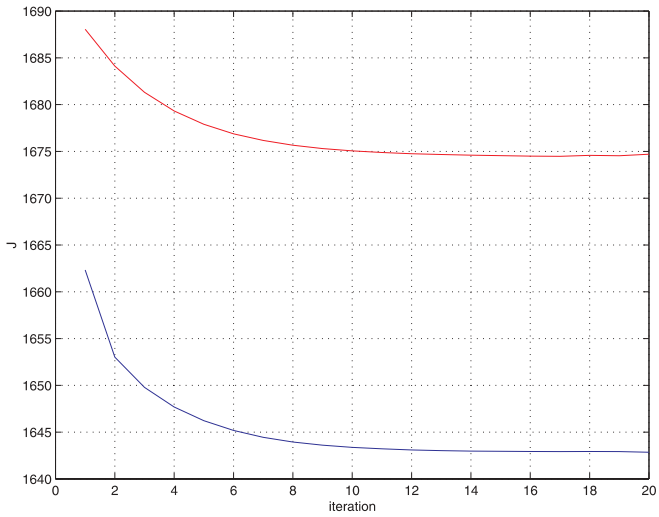

Fig. 7. History of the functional J for the $||\cdot||_1$ norm (*red*) and the $||\cdot||_2$ norm (*blue*)

Table 1. Rates of convergence for a $V(2,2)$-Cycle with initial guess z, for the images depicted in Fig. 1

TV-Norm	$\|\cdot\|_1$	$\|\cdot\|_2$	$\|\cdot\|_1$	$\|\cdot\|_2$
Relaxation	ALR(0.8)		pGS(0.8)	
$\beta = 10^4$	0.87	0.83	n.c.	n.c.
$\beta = 10^5$	0.44	0.27	0.79	0.68
$\beta = 10^6$	0.19	0.13	0.54	0.50
Relaxation	ALR(1.0)		pGS(1.0)	
$\beta = 10^4$	0.66	0.62	n.c.	n.c.
$\beta = 10^5$	0.35	0.18	0.73	n.c.
$\beta = 10^6$	0.11	0.06	0.42	0.37
Relaxation	ALR(1.3)		pGS(1.3)	
$\beta = 10^4$	0.79	0.47	n.c.	n.c.
$\beta = 10^5$	0.29	0.10	0.69	0.68
$\beta = 10^6$	0.03	0.02	0.27	0.20

order. The best convergence rates are observed for the over-relaxed ALR by using the $||\cdot||_2$ norm. Due to the fact that the discretization operator $L_h^{[1]}$ in general is more anisotropic than $L_h^{[2]}$ the rates for the $||\cdot||_2$ norm are better than the rates for the $||\cdot||_1$ norm.

We conclude that the nonlinear multigrid method with ALR relaxation, as presented in this section, is a robust and efficient numerical method for solving the Euler–Lagrange equation (4) for a particular β with unknown size. On the other hand the quality of a minimizer u of the functional $J_{\alpha,\beta}$ depends significantly on the choice of the smoothing parameter β. Theoretically, decreasing β should give a reconstruction of the steep edges in u. Increasing β leads to multigrid schemes with good convergence rates. The aim of the next section is to overcome this problem and to develop a method for the efficient and robust solution of the image denoising problem.

The observed multigrid convergence rates are much worse than for model problems due to several difficulties. First, the problem has highly jumping coefficients. Additionally the coefficients are approximately $\mathcal{O}(h)$ near steps so that one observes the same difficulties as for artificial viscosity discretizations (see, e.g. [20]).

4 Iterative total variation regularization

In the previous section we have described a nonlinear multigrid algorithm which computes an approximation of a minimizer of the functional (3) for a given smoothing parameter β. To recover an image with homogeneous zones and sharp variations at edges, we have to choose a β small compared to u_x^2 and u_y^2. Unfortunately, the smaller β the more degenerated is the differential operator $\mathcal{L}$ and the solution of the PDE by a multigrid method becomes delicate (e.g., see Table 1). On the other hand the larger β the more isotropic ("smoother") is the problem, but the resulting images hold smooth edges.

To overcome this problems, in this section we present an approach, which is closely related to the iterative Tikhonov regularization method [12, 13, 18]. We solve a sequence of minimization subproblems

$$u_{\beta_k}^{(k+1)} = \arg\min_u \left\{ \left|u^{(k)} - z\right|^2 + \alpha \operatorname{div}\left(\frac{\nabla u^{(k)}}{\sqrt{|\nabla u^{(k)}|^2 + \beta_k}}\right)\right\} \tag{7}$$

with decreasing $\beta_k \to 0$ for $k \to \infty$. The solution is determined by calculating the approximations for a exponentially decreasing sequence of parameters $\beta_{k+1} = \beta_k \cdot \kappa$ with a factor $\kappa \in (0,1)$ and a sufficiently large β_0. As initial guess $u^{(0)}$, we use the noisy image z. The solutions $u = u^{(k+1)}$ crucially depend on the choice of the parameter $\beta_k > 0$. Each subproblem is well posed for β sufficiently large and can be solved by the proposed FAS efficiently. For smaller β the problem is still anisotropic but by the use of the smooth initial guess $u^{(k)}$ the problem becomes solvable. We get the following algorithm:

Algorithm 1 Iterative *TV* Regularization.

1: **function** DENOISE (z, u)
2: $\quad k \leftarrow 0$

3: $u^{(k)} \leftarrow z$
4: $\beta_0 \leftarrow M(\gg 0)$
5: **repeat**
6: solve (4) approximately by a FAS
7: $\beta_{k+1} = \kappa^k \cdot \beta_0$
8: **until** $\dfrac{TV\left[u^{(k+1)}\right] - TV\left[u^{(k)}\right]}{TV\left[u^{(k)}\right]} \leq \varepsilon$
9: $u \leftarrow u^{(k)}$
10: **end function**

5 Experimental results

In this section results are given that demonstrate the performance of the iterative total variation regularization based on a nonlinear multigrid scheme. The first test image shown in Fig. 1 (left) is a part of the emblem of the Heinrich-Heine University Düsseldorf. The image consists of 128×128 picture elements. Figure 1 (right) displays the original image degraded by Gaussian noise. The images shown in Fig. 3 are the results of the iterative *TV* regularization (Algorithm 1) by using $\alpha = \kappa = \frac{1}{2}$ and $\beta_0 = 10^4$ as well as a FAS *V*-cycle with maximum number of coarse grids (i.e. seven grids), one pre and one post smoothing step by the ALR applied with an over-relaxing parameter $\omega = 1.3$ and the grid transfer functions as described in Sect. 3.3.1. Differences between the two results are hardly visible to the naked eye. Therefore in the Figs. 4–6, we present the gray-values of the 60-th row in the noisy image and in the resulting images for the two used norms. Comparing the graph displayed in Fig. 5 with the graph for the $||\cdot||_2$ norm in Fig. 6 shows that sharp edges in the images could be restored better by the iterative *TV* regularization algorithm when using the $||\cdot||_1$ norm. These

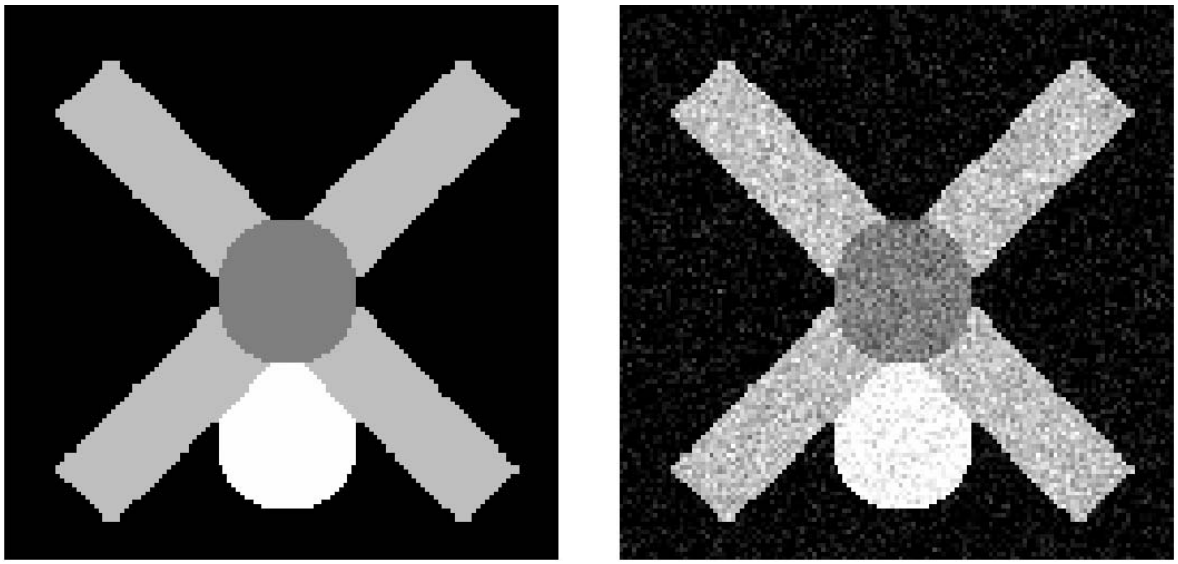

Fig. 8. *Left:* Original image u (128×128) pixels. *Right:* Image $z = u +$ Gaussian white noise

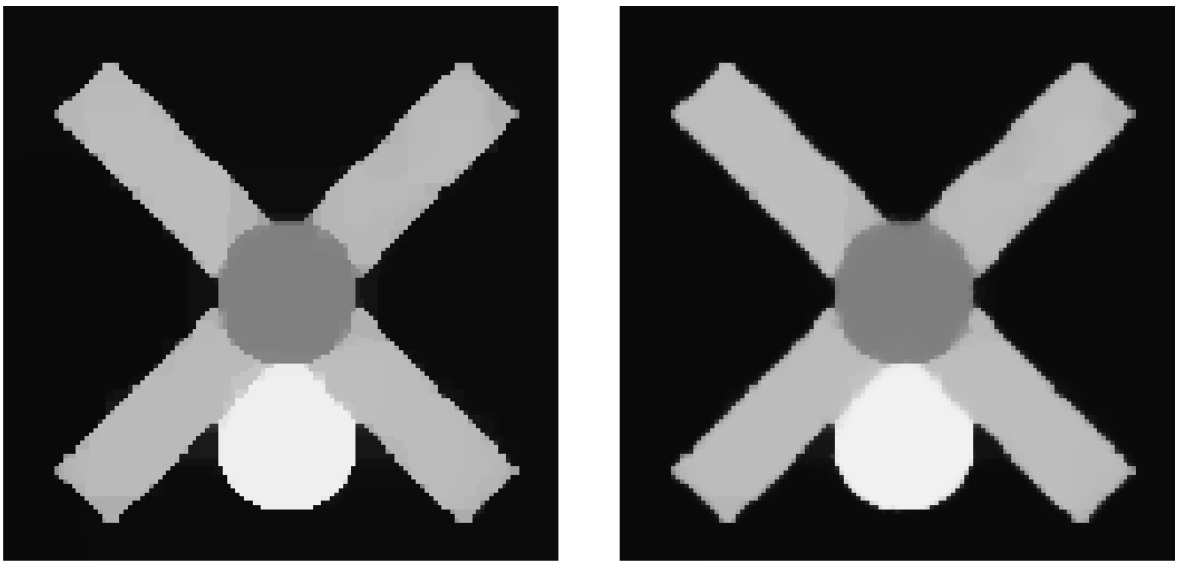

Fig. 9. Result found with iterative total variation regularization. *Left*: By using $||\cdot||_1$. *Right*: By using $||\cdot||_2$

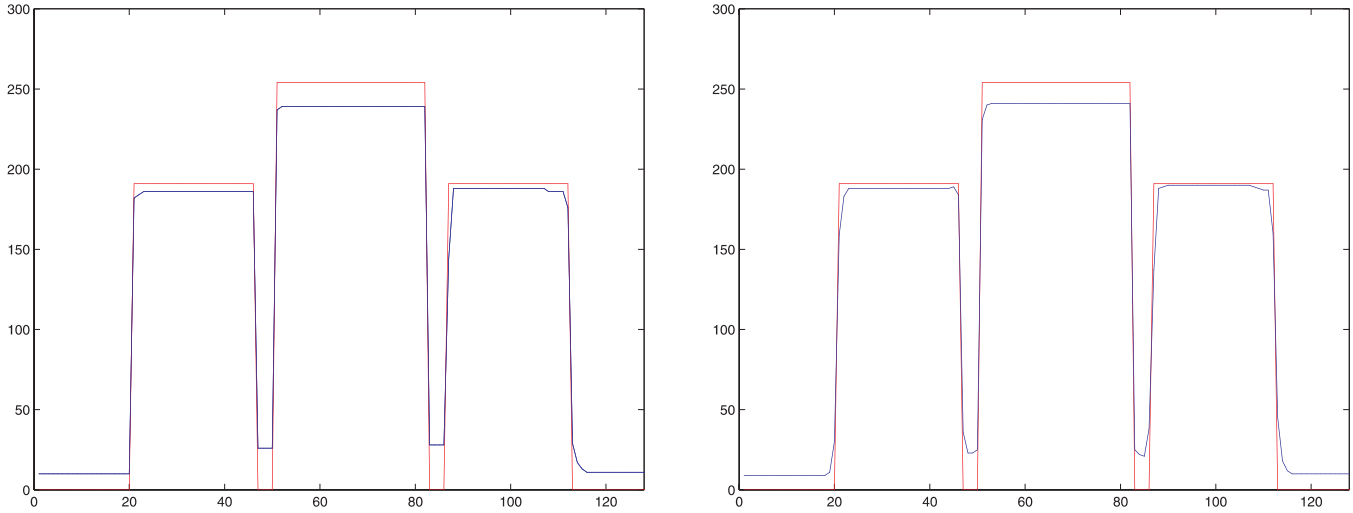

Fig. 10. Functional representation of the image row 100 of the original image (*red*) and the result (*blue*) displayed in Fig. 9. *Left:* By using $||\cdot||_1$. *Right*: By using $||\cdot||_2$

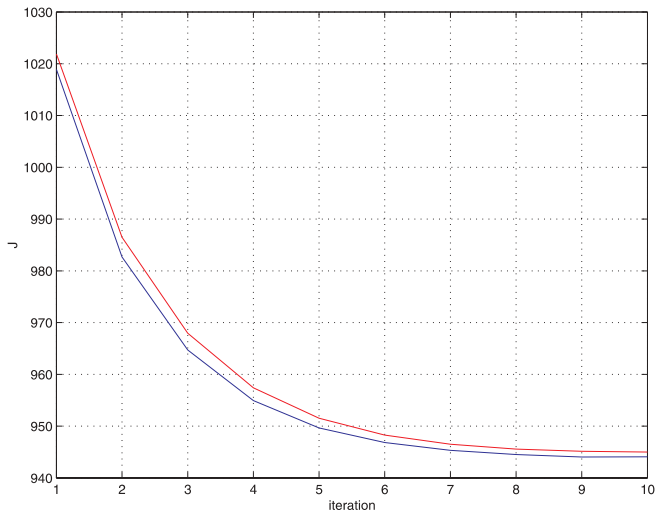

Fig. 11. History of the functional J for the $||\cdot||_1$ norm (*red*) and the $||\cdot||_2$ norm (*blue*)

findings can be stressed by the graph in Fig. 7. Here, the decreasing functionals J for the two norms are displayed. The graphs show the decreasing values of the energy-functional J during the iteration. The iteration using the $||\cdot||_2$ norm actually converges toward a value with a larger magnitude than in the $||\cdot||_1$ case.

The same behavior of the algorithm concerning the norms is observed for the next example depicted in Fig. 8 with corresponding results in Fig. 9.

References

1. Acar, R., Vogel, C.: Analysis of bounded variation penalty method. Inverse Problems 10, 1217–1229 (1994)
2. Baumeister, J.: Stable Solution of Inverse Problems. Vieweg Advanced Lectures 1987
3. Brandt, A.: Multi-level adaptive solutions to boundary value problems. Math. Comp. 31, 333–390 (1977)
4. Brandt, A.: Multigrid techniques: Guide with applications to fluid dynamics. GMD-Studie Nr. 85, GMD, St. Augustin, 1984
5. Chambolle, A., Lions, P.-L.: Image recovery via total variation minimization and related problems. Numer. Math. 76, 167–188 (1995)
6. Chan, T., Chan, R., Zhou, H.: A continuation method for total variation denoising problems. In: Proceedings of the SPIE Conference on Advanced Signal Processing Algorithms, 1995
7. Chan, T.F., Golub, G.H., Mulet, P.: A nonlinear primal-dual method for total variation-based image restoration. In: ICAOS '96 (Paris, 1996), Vol. 219, Berlin, Germany / Heidelberg, Germany / London, UK / etc.: Springer-Verlag 1996, pp. 241–252
8. Coifman, R.R., Sowa, A.: New methods of controlled total variation reduction for digital functions. SIAM Journal on Numerical Analysis 39, 480–498 (2001)
9. Courant, R.: Calculus of variations. New York, NY: Courant Institute of Mathematical Sciences 1962
10. Engl, H.W., Hanke, M., Neubauer, A.: Regularization of Inverse Problems. Dordrecht, The Netherlands: Kluwer Academic Publishers 1996
11. Hackbusch, W.: Elliptic Differential Equations, Theory and Numerical Treatment, Springer Series in Computational Mathematics 18. Berlin Heidelberg New York: Springer-Verlag 1992
12. Hanke, M., Groetsch, C.: Nonstationary iterated tikhonov regularization. J. Optim. Theory and Applications 98, 37–53 (1998)
13. Henn, S., Witsch, K.: Iterative multigrid regularization techniques for image matching. SIAM J. Sci. Comput. (SISC) 23(4), 1077–1093 (2001)
14. Li, Y., Santosa, F.: A computational algorithm for minimizing total variation in image restoration. IEEE Trans. Image Proc. 5, 987–995 (1996)
15. Oman, M: Fast multigrid techniques in total variation-based image reconstruction. In: Proceedings of the 1995 Copper Mountain Conference on Multigrid Methods, 1995
16. Radmoser, E., Scherzer, O., Schöberl, J.: A cascadic algorithm for bounded variation regularization
17. Rudin, L., Osher, S., Fatemi, E.: Nonlinear total variation-based noise removal algorithms. Physica D 60, 259–268 (1992)
18. Scherzer, O., Weickert, J.: Relations between regularization and diffusion filtering. 1998
19. Stüben, K., Trottenberg, U.: Multigrid methods: Fundamental algorithms, model problem analysis and applications. Springer Verlag, Lecture Notes in Mathematics 960, (1982)
20. Trottenberg, U., Osterlee, C., Schüller, A.: Multigrid. Academic Press 2000
21. Vassilevski, P.S., Wade, J.G.: A comparison of multilevel methods for total variation regularization. Elect. Trans. Numer. Anal. 6, 255–270 (1997)
22. Vogel, C.: Computational Methods for Inverse Problems. Frontiers in Applied Mathematics, Philadelphia: SIAM 2002
23. Vogel, C.R., Oman, M.E.: Iterative methods for total variation denoising. SIAM Journal on Scientific Computing 17, 227–238 (1996)